Reac Kinet Mech Cat (2015) 115:773–786
DOI 10.1007/s11144-015-0870-z

Ultrasonic-assisted facile synthesis of plasmonic Ag@AgCl cuboids with high visible light photocatalytic performance for Rhodamine B degradation

Wei-Li Dai[1] · Hai Xu[1] · Li-Xia Yang[1] · Xu-Biao Luo[1] · Xin-Man Tu[1] · Yan Luo[1]

Received: 8 February 2015 / Accepted: 2 April 2015 / Published online: 12 April 2015

Abstract Using amino acids as shape-directing and reducing agents, a plasmonic photocatalyst of Ag@AgCl cuboids is rapidly prepared through a one-step ultrasonic-assisted approach. By controlling the species of amino acid, the Ag^0 content on the AgCl surface and surface plasmon resonance (SPR) adsorption of Ag@AgCl can be rationally tailored simultaneously, which are responsible for the excellent photocatalytic activity of Ag@AgCl photocatalysts. Among the as-synthesized Ag@AgCl samples, the Ag@AgCl-Lys synthesized by using L-lysine had the highest Ag^0 content and showed the best photocatalytic activity for the degradation of Rhodamine B (RhB) and formic acid (FA) under visible light irradiation. In addition, the Ag@AgCl photocatalyst exhibited good stability and recyclability. After 5 runs, Ag@AgCl-Lys did not have any significant loss of activity. Moreover, the photocatalytic mechanism was investigated by active species-trapping experiments, which shows that the $\cdot O_2^-$ is the main reactive species for the degradation of RhB. This study may provide a novel strategy for design and preparation of advanced visible light sensitized photocatalysts.

Keywords Plasmonic Ag@AgCl · Ultrasonic-assisted · Amino acid · Photodegradation

Electronic supplementary material The online version of this article (doi:10.1007/s11144-015-0870-z) contains supplementary material, which is available to authorized users.

✉ Wei-Li Dai
wldai81@126.com; daiweili@nchu.edu.cn

[1] Key Laboratory of Jiangxi Province for Persistant Pollutants Control and Resources Recycle, College of Environmental and Chemical Engineering, Nanchang Hangkong University, Nanchang 330063, Jiangxi, China

Introduction

Semiconductors as photocatalysts are expected to play an increasingly important role in many applications for the utilization of solar energy, for example, the conversion of water to hydrogen gas by photocatalytic water splitting [1], the creation of self-cleaning surfaces [2], disinfection of water [3], degradation of organic contaminants [4], as well as photoreduction of CO_2 to gaseous hydrocarbons [5, 6]. As a traditional and most popular photocatalyst, TiO_2 has been extensively used and investigated. However, the visible light photocatalytic activity of TiO_2 is limited because of the wide band gap of 3.2 eV [7, 8]. Although many methods such as impurity doping [9], metallization [10], and sensitization [11] have been applied to TiO_2 to extend the photoresponsive range towards the visible light, high synthesis cost and processing complexity limited enhancement in photocatalytic efficiency make them less appealing for widespread commercial application. Thus, it is highly desirable to develop a simple method to prepare the catalysts with high stability, high activity, low-cost and strong visible light response.

In the past decades, nanoscaled noble metals (such as silver and gold) have been extensively studied due to their unique surface plasmon resonance (SPR) properties in the visible region and a relative low Fermi level, which could decrease the recombination of photogenerated electrons and holes. Therefore, noble metal nanoparticles (NPs) could be utilized as a kind of visible light harvesting and converting centers to develop new plasmon enhanced photocatalysts. For example, the Au (or Ag)-loaded TiO_2 [12], WO_3 [13], ZnO [14], AgX (X=Cl, Br, I) [15], and other large-bandgap semiconductors [16] exhibit high photocatalytic performance in the visible light region. Recently, Ag@AgCl plasmonic photocatalysts, consisting of silver salt particles decorated with in situ grown Ag NPs, have been developed into promising photocatalysts for environmental purification applications under sunlight or visible light irradiation [17, 18]. It is well known that the AgCl NPs exhibit strong absorption only in the ultraviolet spectral region and weak absorption in the visible region due to the large bandgaps, direct bandgap of 5.15 eV (241 nm) and an indirect bandgap of 3.25 eV (382 nm) [17]. Nevertheless, (as for Ag^0) the electric fields around silver NPs can be enhanced when the incident lights are in the resonance with the localized surface plasmon of silver NPs [19–21]. Hence it is an effective way to improve the photocatalytic activity of AgCl by constructing Ag@AgCl. Huang et al. [22] first synthesized Ag@AgCl as plasmonic photocatalyst by an ion exchange reaction between aqueous solutions of Ag_2MoO_4 and HCl followed by UV irradiation. Since then, Ag@AgCl as a promising plasmonic photocatalyst was further studied and developed. For example, multistep thermal polyol process [23], microwave-assisted [24], and sonochemical polyol techniques [25] were developed for the synthesis of Ag@AgCl particles with good photocatalytic activity. However, most of those methods mentioned above are time consuming, cost-intensive, and/or they have to be carried out under elevated temperatures, which do not meet the synthetic requirement of green chemistry in modern science. Consequently, new and simple approach for rapid synthesis of plasmonic Ag@AgCl photocatalyst is needed to be developed.

Besides synthetic macromolecular compounds such as sodium dodecylbenzene sulfonate (SDBS), polyvinylpyrrolidone (PVP), and cetyltrimethylammonium bromide (CTAB), some biomolecules employed as eco-friendly and inexpensive directing agents and/or capping agents for the synthesis of photocatalytic materials have attracted much attention in the past few years. Amino acids are promising and interesting biomolecular surfactants due to their multiple functional groups and adjustable polarity. For example, L-cysteine as a surfactant was widely used in the fabrication of photocatalysts such as ZnO nanorod arrays, flower-like In_2S_3, pagoda-like PbS with hierarchical architectures, NiS microcrystals, and CdS nanoshperes [26–30]. To the best of our knowledge, however, there is no report on the synthesis of Ag@AgCl plasmonic materials by using amino acids as surfactant. Herein, various amino acids were exploited for the first time for the one-pot synthesis of the Ag@AgCl plasmonic photocatalysts under ultrasonic conditions. The readily fabricated Ag@AgCl presents excellent visible light activity for photocatalytic degradation of Rhodamine B (RhB) and Formic acid (FA).

Experimental

Reagents

Silver nitrate ($AgNO_3$), sodium chloride (NaCl), ethylene glycol (EG), L-lysine (Lys), L-valine (Val), L-glutamic (Glu), PVP, ethanol, Rhodamine B, and Formic acid were purchased from Shanghai Jingchun Industry Co., Ltd. All the reagents were used as received without further treatment.

Preparation of photocatalysts

Ag@AgCl photocatalysts were synthesized by a facile and rapid ultrosonic-assisted nonaqueous synthesis route. In a typical procedure, NaCl (300 mg) and the amino acid (225 mg) were added into 100 mL of EG to form a clear solution at room temperature. Then, 8 mL of EG solution containing $AgNO_3$ (510 mg) was added dropwise to the above Cl^--amino acid solution under ultrasonic conditions. A white milky suspension immediately formed after the addition of the Ag^+ solution, and the white suspension gradually became pale red in the sonication duration. The temperature of the suspension during sonication was monitored with a thermometer, and the apparent temperature was 70–80 °C. After reacting for 30 min under ultrasonic conditions, the hybrid particles were cooled down to room temperature, collected by centrifugation, washed three times with alcohol and water, and dried at 80 °C for 12 h. The Ag@AgCl photocatalysts synthesized by using various amino acids, such as L-lysine (Lys), L-valine (Val), and L-glutamic acid (Glu) were denoted as Ag@AgCl-Lys, Ag@AgCl-Val, and Ag@AgCl-Glu.

For comparison, the Ag@AgCl-PVP photocatalyst was synthesized under the same reaction conditions by using PVP to substitute amino acid. Moreover, the Ag@AgCl-Lys-H photocatalyst was synthesized by hydrothermal heating method instead of sonication during the reaction process.

Characterization

Powder X-ray diffraction (XRD) measurements were performed on a Bruker AXS-D8 diffractometer with CuK_α radiation ($\lambda = 0.15{,}418$ nm). UV/Vis absorption spectra were recorded on a Hitachi U-3900H instrument by using $BaSO_4$ as the reference. The morphology was observed with a Nova Nano SEM450 field-emission scanning electron microscopy (SEM). Surface electronic states were analyzed by X-ray photoelectron spectra (XPS, Perkin-Elmer PHI-5300 spectrometer, Al KR). All of the binding energies were calibrated by using the contaminant carbon (C_{1s} 284.6 eV) as a reference.

Photocatalytic activity

The photocatalytic activities of the samples were evaluated by the photocatalytic degradation of RhB and FA aqueous solution at ambient temperature under a 300 W Xe lamp with UV cut off filter ($\lambda \geq 420$ nm). In a typical procedure, 50 mg Ag@AgCl photocatalyst was suspended in 50 mL RhB aqueous solution (10 mg L^{-1}) in a 100 mL beaker. Prior to irradiation, the suspension was stirred for 30 min in the dark to ensure an adsorption/desorption equilibrium between the photocatalyst and RhB dye. During the photocatalytic degradation processes, 2 mL of suspensions were sampled at certain time intervals and centrifuged to remove the photocatalyst particles. The upper clear liquid was analyzed by recording the characteristic absorption peak of RhB at 553 nm with an UV–Vis spectrophotometer to calculate the concentrations of the dye.

The photocatalytic degradation of FA solution (1 mmol L^{-1}) was carried out by the same procedure like that of RhB. The concentration of FA samples was detected by UV–Vis spectrophotometer at 206 nm.

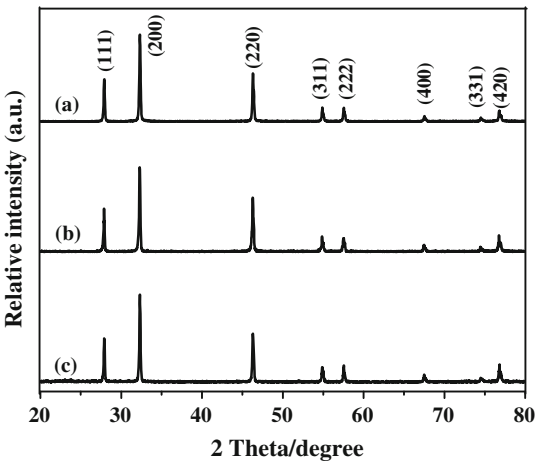

Fig. 1 XRD patterns of **a** Ag@AgCl-Lys, **b** Ag@Ag-Val, and **c** Ag@AgCl-Glu

Photoelectrochemical measurements

Photocurrents were measured using an electrochemical analyzer (CHI660C Instruments) in a standard three-electrode system with the prepared samples as the working electrodes with an active area of catalyst 1.0 cm^2, a graphite as the counter electrode, and SCE (saturated calomel electrode) as a reference electrode. A 300 W Xe lamp equipped with an ultraviolet cut off filter to provide visible light with $\lambda \geq 420$ nm served as the visible light source. A 0.5M Na_2SO_4 aqueous solution was used as the electrolyte.

Results and discussion

Characterization of Ag@AgCl photocatalysts

The XRD patterns of the as-prepared Ag@AgCl photocatalysts are shown in Fig. 1. All patterns matched very well with the JCPDS standard data of AgCl (JCPDS No. 31-1238), and no impurity phase is found. The diffraction peaks at 2θ values of 27.8, 32.2, 46.2, 54.8, 57.5, 67.5, 74.5 and 76.7° are assigned to the (111), (200), (220), (311), (222), (400), (331) and (420) planes of AgCl, in order. It is noted that there is no reflection assigned to Ag metal in the XRD patterns, possibly because that the low Ag content [31] was below the detection limit and/or the Ag particles on the surface of AgCl are poorly crystallized [32, 33]. Furthermore, the intensity ratio of I_{200}/I_{111} for the Ag@AgCl samples is about 2.2, 2.06, 2.16, which is synthesized by using different amino acids (Lys, Val, Gul). These results are higher than the literature data (JCPDS No.31-1238) of $I_{200}/I_{111} = 2.0$. It was reported that the oxygen atoms of PVP preferentially bind to (100) crystallographic planes of FCC silver, which can inhibit AgCl (100) faces and reduce the area of (111) faces during the growth of AgCl cubic crystals [34]. It is envisioned that the oxygen atoms of amino acid could play the similar role like that of PVP. Therefore, the AgCl cuboids were obtained by joining amino acids as directing and assembling agent [35].

The morphologies of the as-synthesized Ag@AgCl photocatalysts were observed by SEM. As shown in Fig. 2, all the Ag@AgCl particles synthesized by using

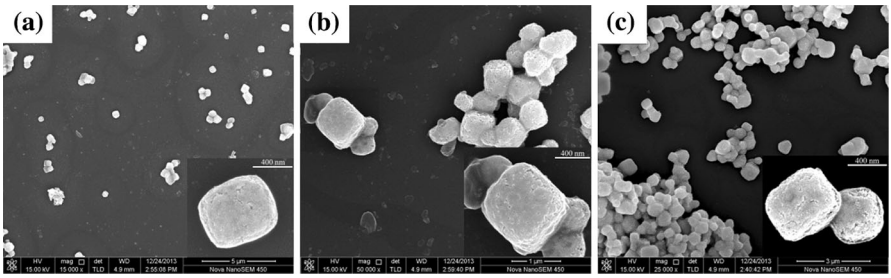

Fig. 2 SEM images of **a** Ag@AgCl-Lys, **b** Ag@AgCl-Val, and **c** Ag@AgCl-Glu

various amino acids have a cuboid shape and uniform sizes, which is consistent with the results of XRD.

The elemental composition, chemical status and silver (Ag^0) content of the Ag@AgCl sample are further analyzed by means of XPS. The survey spectra (Fig. S1) of the as-synthesized Ag@AgCl samples are similar and confirmed that the Ag and Cl are the main components. In addition, small amounts of O, N, and C are detected. The N 1 s, C 1 s, and O 1 s peaks are attributed to the trace amounts of amino acid molecules adsorbed on the surfaces of Ag@AgCl particles. Ag 3d spectrum (Fig. 3) consists of two peaks at 367.7 and 373.7 eV, which correspond to the binding energies of Ag $3d_{3/2}$ and Ag $3d_{5/2}$, respectively. The two peaks can be further deconvoluted into two different peaks at 367.5 and 368.8 eV, as well as 373.5 and 374.6 eV. The bands at 367.5 and 373.5 eV are attributed to the peaks of Ag^+ (AgCl), and the bands at 368.8 and 374.6 eV could be ascribed to the peaks of metallic Ag^0 [36]. According to the XPS results, the surface Ag^0 contents of the Ag@AgCl-Lys, Ag@AgCl-Val and Ag@AgCl-Glu samples are calculated to be 8.4, 7.9, and 7.3 mol%, respectively. Moreover, two peaks at about 199.6 and 197.9 eV were observed in the Cl 2p spectra (Fig. S2), corresponding to the binding of Cl $2p_{1/2}$ and Cl $2p_{3/2}$ respectively. This illustrates the existence of Cl^-.

From the above results, we can see that the Ag^0 content of the as-synthesized Ag@AgCl samples is in the order of Ag@AgCl-Lys > Ag@AgCl-Val > A-g@AgCl- Glu. Xu et al. [37] considered that PVP not only acted as a growth controlling agent but also as a reducing agent to reduce partial Ag^+ to metallic Ag in the synthesis process of Ag@AgBr samples. Herein, we speculate that the amino acids also play similar roles, acting as both a shape-directing agent for the synthesis of AgCl cuboids and a reducing reagent for the formation of Ag^0 in the synthesis process of Ag@AgCl photocatalysts. Meanwhile, the amino acid molecules with more amino groups could exhibit stronger reducing ability. Accordingly, the reducing ability of the amino acids is in the order of L-lysine > L-valine >

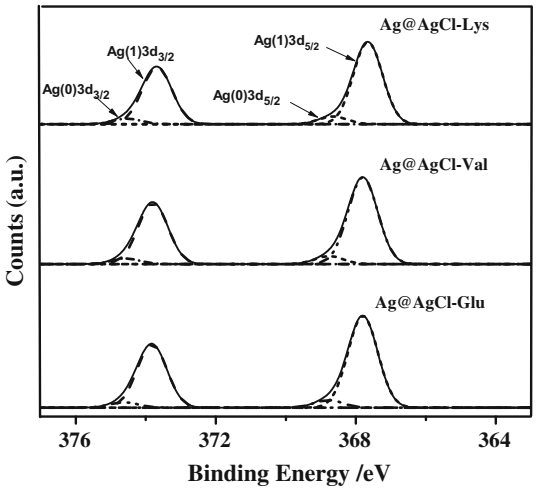

Fig. 3 XPS spectra of Ag 3d in the as-prepared Ag@AgCl samples

L-glutamic acid, which is in consistent with the Ag^0 content trend in corresponding Ag@AgCl samples.

Fig. 4 shows the UV/Vis absorption spectra of AgCl and Ag@AgCl samples. For pure AgCl, only a peak in the range of 350–400 nm can be observed, which is consistent with the previous report [38]. However, Ag@AgCl samples have strong absorption both in the ultraviolet and visible light regions. The absorption at 350–400 nm can be ascribed to the characteristic absorption of AgCl, and the strong absorption in the region of 400–800 nm can be attributed to the typical SPR of metallic Ag NPs [39]. Compared with Ag@AgCl-Val and Ag@AgCl-Glu, the band of Ag@AgCl-Lys in the visible light region shows a red shift and broadening. Generally, the resonance wavelength strongly depends on the size and shape of the NPs, the interparticle distance, and the dielectric property of the surrounding medium [24]. Here, the increase of the Ag to AgCl ratio with the ordinal use of L-lysine, L-valine, and L-glutamic acid may be responsible for this unique phenomenon.

Photocatalytic activities of Ag@AgCl photocatalysts

In order to investigate the photocatalytic activities of the as-synthesized Ag@AgCl samples and the role of SPR effect during the photocatalysis process, the degradation of RhB aqueous solution (10 mg L^{-1}) under visible light irradiation ($\geq$420 nm) was evaluated. Fig. 5 shows the photodegradation curves of RhB over different photocatalysts. A blank experiment in the absence of the photocatalyst but under visible light irradiation shows that no RhB has been decomposed. Another blank experiment using Ag@AgCl-Lys as photocatalyst without being irradiated demonstrated that the concentration of RhB remained unchanged (not shown in Fig. 5). Those results indicated that the RhB is very stable, and the possible catalytic degradation of RhB over Ag@AgCl-Lys in the dark is excluded. Further control experiments showed that RhB was not photocatalytically degraded on bare Ag NPs.

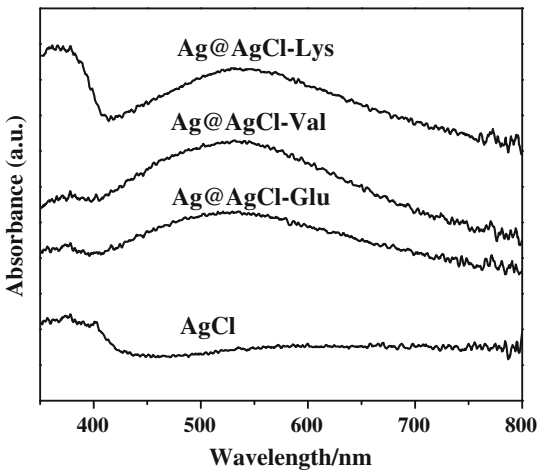

Fig. 4 UV/vis absorption spectra of AgCl and the as-synthesized Ag@AgCl samples

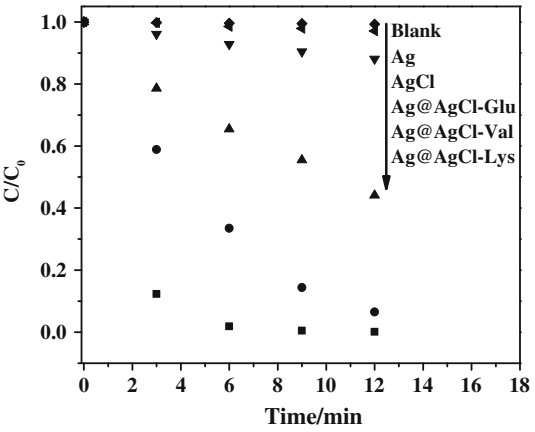

Fig. 5 Photocatalytic degradation of RhB over various photocatalysts under visible light irradiation (≥420 nm). Experimental conditions: catalyst dosage = 50 mg, volume of solution = 50 mL, initial concentration = 10 mg L^{-1}

This confirms that the local dielectric environment for Ag NPs is crucial for plasmonic photocatalysis and rules out a surface plasmon induced localized heating effect of Ag NPs for the degradation of RhB as well [40]. Furthermore, a bare AgCl showed very poor visible light driven photocatalytic activity, due to its large indirect band gap (3.25 eV). However, the loading of Ag NPs on the AgCl surface remarkably enhanced the RhB degradation efficiency over the Ag@AgCl samples. It can be seen that the RhB was completely decomposed over Ag@AgCl-Lys within 6 min. Moreover, Ag@AgCl-Val and Ag@AgCl-Glu all exhibited much higher photocatalytic activity than the bare Ag NPs and AgCl. Therefore, the excellent visible light photocatalytic performance of Ag@AgCl may be ascribed to the interfacial interaction between Ag and AgCl. Interestingly, the trend in the photocatalytic activities of the as-synthesized samples follows the order of Ag@AgCl-Lys > Ag@AgCl-Val > Ag@AgCl-Glu, which is in consistent with the order of the Ag^0 contents of those samples. This phenomenon can be interpreted as the higher metallic Ag content which increase the density of Ag NPs on the surface of AgCl particles and improve their interface area. This favors the electron–hole separation and interfacial charge transfer [22], which finally enhances the photocatalytic performance of the Ag@AgCl samples. The results suggest that the photocatalytic activities of Ag@AgCl can be rationally tailored by controlling the species of amino acid in the synthesis process. In order to rule out the photosensitization process of the Ag@AgCl photocatalysts, FA was chosen as a colorless model organic pollutant. As shown in Fig. S3, it can be seen that when the parent bare Ag NPs and AgCl are used as photocatalysts, no more than 5 % and 10 % FA, respectively, are decomposed within 40 min under visible light irradiation. While the as-synthesized Ag@AgCl are employed as photocatalysts, they show significantly enhanced photocatalytic activity than that of bare Ag NPs and AgCl. Furthermore, it is found that the photocatalytic activity of the Ag@AgCl samples are enhanced in the order of Ag@AgCl-Lys > Ag@AgCl-Val > Ag@AgCl-Glu, which is consistent with the results of RhB photodegradation. From the results, it can see that the Ag@AgCl as plasmonic photocatalysts exhibit

good photocatalytic activity for the degradation of both dyes and colorless organic pollutants.

The photodegradation process of RhB was found to follow pseudo-first order kinetics. As shown in Fig. 6, the rate constant for the Ag@AgCl-Lys was evaluated as 0.5733 min^{-1}. In many reports [23, 25, 36], PVP was usually used for the synthesis of Ag@AgCl or other photocatalysts. In comparison, Ag@AgCl-PVP was synthesized by using PVP, and was evaluated in the degradation of RhB dye. It was found that the rate constant of Ag@AgCl-PVP is 0.3980 min^{-1}, which is much lower than that of Ag@AgCl-Lys. Furthermore, the photocatalysts of Ag@AgCl-Lys-H and Ag@AgCl-PVP-H synthesized by traditional hydrothermal method were also studied, whose rate constants are 0.2250 and 0.1350 min^{-1}, respectively. Obviously, the Ag@AgCl-Lys exhibited outstanding photocatalytic performance than the above photocatalysts. Hence, this study provides a valuable strategy for the synthesis of effective, low-cost, and eco-friendly visible light SPR Ag@AgCl photocatalyst.

The stability and recyclability of a photocatalyst is very important for its application. Hence, the stability and recyclability of plasmonic photocatalyst Ag@AgCl-Lys was further investigated by reusing it in the photodegradation of RhB dye. As shown in Fig. S4, RhB is quickly decomposed catalyzed by Ag@AgCl-Lys. The Ag@AgCl-Lys photocatalyst is stable after 5 runs exhibiting no significant loss of activity.

Photocatalytic mechanism

In the photocatalytic oxidation process, electron–hole pairs are directly produced on the photocatalyst surface after illumination. Consequently, a series of photoinduced reactive species including h^+, ·OH, and $\cdot O_2^-$ are generated and commonly suspected to be involved in the photocatalytic degradation of organic pllutants.

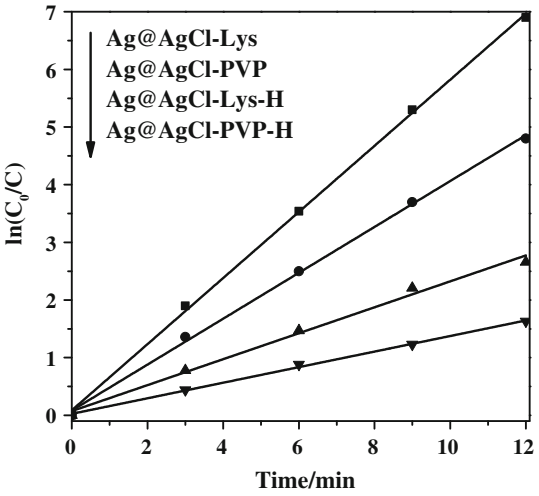

Fig. 6 Kinetic rate plots of RhB degradation over various photocatalysts synthesized by different methods under visible light irradiation (≥420 nm). Experimental conditions: catalyst dosage = 50 mg, volume of solution = 50 mL, initial concentration = 10 mg L^{-1}

Jiang et al. [31] reported that the direct photohole mainly worked as reactive radical species for the oxidation of organic pollutant molecules over Ag@AgCl photocatalyst. Yu et al. [32] reported that the ·OH were active species and indeed participated in phtotocatalytic reactions over Ag/AgCl/TiO_2 composites. Nevertheless, Luo et al. [41] regarded that the active species such as ·OH and $\cdot O_2^-$ all can decompose the adsorbed organic pollution when using Ag/AgCl/rGO as photocatalyst. In order to investigate the photodegradation mechanism in our photocatalytic system, a series of radical- and hole-trapping experiments were designed and carried out over Ag@AgCl-Lys under indoor artificial daylight irradiation. We employed various scavengers to quench these primary active species, i.e., KI as a quencher of h^+ and ·OH, isopropanol (IPA) as a quencher of ·OH, benzoquinone (BQ) as a quencher of $\cdot O_2^-$. The sacrificial agents can capture corresponding radical species, i.e., KI–h^+ + ·OH, IPA–·OH, and BQ–$\cdot O_2^-$, which lead to the lower concentration of reactive species to react with the RhB dye in the solution. The depression effects on RhB degradation by adding different quencher are shown in Fig. 7. It can be observed that the addition of KI and IPA almost did not affect the degradation efficiency of RhB throughout the experiments. Meanwhile, the degradation rates of RhB were significantly reduced after the addition of BQ. The results indicate that $\cdot O_2^-$ may be the main reactive species for the degradation of RhB, rather than h^+ and ·OH. Because the generation of $\cdot O_2^-$ may occur by direct reaction of the photogenerated electrons with O_2 adsorbed on the catalyst surface, an anaerobic experiment was therefore conducted to elucidate the effect of oxygen. It was found that the degradation efficiency of RhB was largely depressed by purging of Ar in the reaction process. This further verifies that $\cdot O_2^-$ maybe act the main reactive species in the photodegradation of RhB over Ag@AgCl-Lys photocatalyst.

Based on the above experiments results, an illustration of the Ag@AgCl formation and photocatalytic mechanism is depicted in Fig. S5. Under visible light illumination, Ag@AgCl nanocomposite has a strong absorption in the visible light region due to SPR effect of Ag NPs, generating a certain number of electron–hole pairs. Because of the synergistic effect between the excellent conductivity of Ag

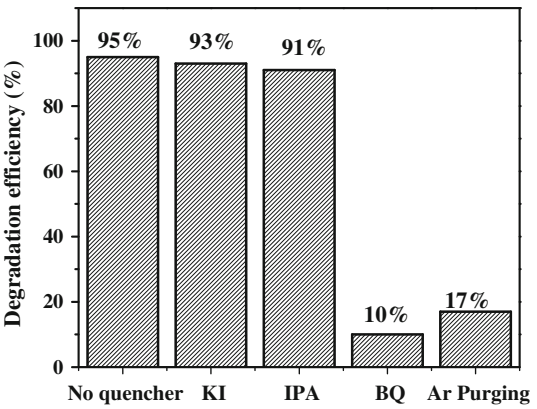

Fig. 7 Degradation efficiency of Ag@AgCl-Lys with different quenchers and by Ar purging under visible light irradiation (≥420 nm). Experimental conditions: catalyst dosage = 50 mg, volume of solution = 50 mL, initial concentration = 10 mg L^{-1}

NPs and the polarization field provided by AgCl, the photogenerated electrons are transferred to the surface of the Ag NPs far from the Ag@AgCl interface and trapped by oxygen molecules in the solution to form superoxide ions ($\cdot O_2^-$), which will oxidize RhB dye molecules. Meanwhile, the photogenerated holes are transferred to the AgCl surface causing the oxidation of Cl^- ions to Cl^0 atoms, which may be another active species to oxidize RhB molecules [24, 25, 38] and hence the Cl^- will be formed again. On the other hand, the quick migration of photogenerated electrons from the AgCl surface will prevents the photoreduction of AgCl to Ag^0. In addition, the recycle of Cl^- ions may be the main factors for the high stability of the as-synthesized photocatalyst [39].

Transient photocurrent response

Photoinduced e^-–h^+ generation, separation, migration and capture by reactive species is considered to be the basic process in semiconductor photocatalyst operation. Photoelectrochemistry tests are powerful tools to monitor these complicated processes. To give further evidence to show the plasmonic enhancements of photocatalytic activity, the photoresponses of the as-synthesized Ag@AgCl and AgCl samples were studied. As shown in Fig. 8, large and rapid anodic photocurrent responses from the light-on to the light-off state can be detected over all Ag@AgCl electrodes, which are mainly ascribed to the quick separation and transportation of photogenerated electrons on the surfaces of working electrodes [42]. The photocurrent response of the samples is in the order of Ag@AgCl-Lys > Ag@AgCl-Val > Ag@AgCl-Glu > AgCl, which is consistent with the order of their photocatalytic activity and Ag^0 content in Ag@AgCl samples. It is regarded that the synergy effects between the SPR of the Ag NPs and the polarization field of AgCl matrix make the the exited surface electron transferring from the Ag NPs to the Ag–AgCl interfaces [43]. This interaction facilitates electron–hole separation and interfacial charge transfer, which is beneficial for the generation of photocurrent and the creation of reactive species $\cdot O_2^-$. In the Ag@AgCl samples, more Ag^0 NPs

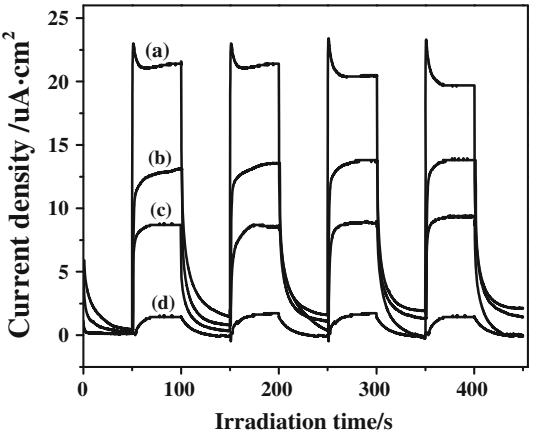

Fig. 8 Transient photocurrent response of **a** Ag@AgCl-Lys, **b** Ag@Ag-Val, **c** Ag@AgCl-Glu, and **d** Ag@AgCl under visible light irradiation (≥420 nm). Experimental conditions: SCE (saturated calomel electrode) as a reference electrode, 0.5M Na_2SO_4 aqueous solution as the electrolyte

on the surface of AgCl means a stronger interaction between the Ag^0 NPs and AgCl matrix. Hence, the as-synthesized SPR photocatalysts of Ag@AgCl show consistent trend with the Ag^0 content, photocurrent response as well as photocatalytic activity. Meanwhile, the photocurrents over Ag@AgCl electrodes were maintained at constant levels throughout the entire experimental period, which confirmed that the Ag@AgCl electrodes have photoactivity and steady photoelectrochemical performance under visible light illumination. Moreover, the photocurrent results also provide a direct evidence for the photocatalytic mechanism.

Conclusion

In summary, we have developed a simple, one-step, effective ultrasonic-assisted approach for the rapid synthesis of Ag@AgCl photocatalysts in an amino acid-EG reaction medium. The composition and SPR adsorption of Ag@AgCl system can be readily modulated by changing the species of amino acid. The synergistic effects between SPR of Ag^0 NPs and the polarization fields of AgCl particles facilitate the separation of photoexcited e^-–h^+ pairs and interfacial charge transfer, thus enhance the photocatalytic activity. Hence, the as-synthesized Ag@AgCl photocatalysts showed excellent photocatalytic performance for the degradation of RhB and FA under visible light irradiation, especially the Ag@AgCl-Lys synthesized by using L-lysine. In addition, Ag@AgCl-Lys showed good stability and recyclability in the photodegradation reaction. Furthermore, the possible degradation mechanism of the plasmonic photocatalytic process was systematically investigated. The active specie $\cdot O_2^-$ is proved to play the most important role in the photodegradation of organic pollutants. It is believed that the obtained Ag@AgCl plasmonic photocatalysts with strong adsorption in the visible light region, the high photocatalytic activity and good photostability have potential applications in the degradation of organic contaminations and environmental cleaning.

Acknowledgments This work was financially supported by the National Natural Science Foundation of China (Grant Nos. 51104089, 51238002, and 51272099). Natural Science Foundation of Jiangxi Provincial Department of Education (Grant Nos. GJJ14537 and GJJ14516).

References

1. Liu Z, Hou W, Pavaskar P, Aykol M (2011) Plasmon resonant enhancement of photo-catalytic water splitting under visible illumination. Nano Lett 11:1111–1116
2. Zhao ZG, Miyauchi M (2008) Nanoporous-walled tungsten oxide nanotubes as highly active visible-light-driven photocatalysts. Angew Chem Int Ed 37:7031–7249
3. Wei C, Lin WY, Zainal Z, Williams NE (1994) Bactericidal activity of TiO_2 photo-catalyst in aqueous media: toward a solar-assisted water disinfection system. Environ Sci Technol 28:934–938
4. Asahi R, Morikawa T, Ohwaki T, Aoki K, Taga Y (2001) Visible-light photocatalysis in nitrogen-doped titanium oxides. Science 293:269–271

5. Varghese OK, Paulose M, LaTempa TJ (2009) High-rate solar photocatalytic conver- sion of CO_2 and water vapor to hydrocarbon fuels. Nano Lett 9:731–737
6. Inoue T, Fujishima A, Honda K, Konishi S (1979) Photoelectrocatalytic reduction of carbon dioxide in aqueous suspensions of semiconductor powders. Nature 277:637–638
7. Yu HG, Irie H, Shimodaira Y, Hosogi Y (2010) An efficient visible-light-sensitive Fe(III)-grafted TiO_2 photocatalyst. J Phys Chem C 114:16481–16487
8. Yu JG, Yu H, Cheng B (2003) The effect of calcination temperature on the surface microstructure and photocatalytic activity of TiO_2 thin films prepared by liquid phase deposition. J Phys Chem B 107:13871–13879
9. Khan SUM, Al-Shahry M, Ingler WB (2002) Efficient photochemical water splitting by a chemically modified n-TiO_2. Science 297:2243–2245
10. Kumar SG, Devi LG (2011) Review on modified TiO_2 photocatalysis under UV/visible light: selected results and related mechanisms on interfacial charge carrier transfer dynamics. J Phys Chem A 115:13211–13241
11. Gratzel M, Nazeeruddin MK, Deacon GB, Pechy P, Renouar T (2001) Engineering of efficient panchromatic sensitizers for nanocrystalline TiO_2-based solar cells. J Am Chem Soc 123:1613–1624
12. Ding D, Liu K, He S, Gao C, Yin Y (2014) Ligand-exchange assisted formation of Au/TiO_2 schottky contact for visible-light photocatalysis. Nano Lett 14:6731–6736
13. Tanaka A, Hashimoto K, Kominami H (2014) Visible-light-induced hydrogen and oxygen formation over Pt/Au/WO_3 photocatalyst utilizing two types of photoabsorption due to surface plasmon resonance and band-gap excitation. J Am Chem Soc 136:586–589
14. Chen Y, Zeng D, Zhang K, Lu A, Wang L, Peng DL (2014) Au-ZnO hybrid nanoflowers, nanomultipods and nanopyramids: one-pot reaction synthesis and photocatalytic properties. Nanoscale 6:874–881
15. Ma X, Dai Y, Guo M, Huang B (2012) The role of effective mass of carrier in the photocatalytic behavior of silver halide-based Ag@AgX(X=Cl, Br, I): a theoretical study. ChemPhysChem 13:2304–2309
16. Tanaka A, Hashimoto K, Kominami H (2012) Preparation of Au/CeO_2 exhibiting strong surface plasmon resonance effective for selective or chemoselective oxidation of alcohols to aldehydes or ketones in aqueous suspensions under irradiation by green light. J Am Chem Soc 134:14526–14533
17. An C, Ming X, Wang J (2012) Construction of magnetic visible-light-driven plasmonic Fe_3O_4@-SiO_2@AgCl: Ag nanophotocatalyst. J Mater Chem 22:5171–5176
18. An C, Wang R, Wang S, Zhang X (2011) Converting AgCl nanocubes to sunlight-driven plasmonic AgCl: Ag nanophotocatalyst with high activity and durability. J Mater Chem 21:11532–11536
19. Awazu K, Fujimaki M, Rockstuhl C, Tominaga J, Murakami H (2008) A plasmonic photocatalyst consisting of silver nanoparticles embedded in titanium dioxide. J Am Chem Soc 130:1676–1680
20. Wang P, Xie TF, Li HY, Peng L, Zhang Y, Wu TS, Pang S (2009) Synthesis and plasmon-induced charge-transfer properties of monodisperse gold-doped Titania microspheres. Chem Eur J 15:4366–4372
21. Du L, Furube A, Yamamoto H, Hara K, Katoh R, Tachiya M (2009) Plasmon- induced charge separation and recombination dynamics in gold-TiO_2 nanoparticle systems: dependence on TiO_2 particle size. J Phys Chem C 113:6454–6462
22. Wang P, Huang BB, Qin XY, Zhang XY, Dai Y, Wei JY (2008) Ag@AgCl: a highly efficient and stable photocatalyst active under visible light. Angew Chem Int Ed 47:7931–7933
23. An C, Peng S, Sun YG (2010) Facile synthesis of sunlight-driven AgCl: Ag plasmonic nanophotocatalyst. Adv Mater 22:2570–2574
24. Jiang J, Zhang LZ (2011) Rapid microwave-assisted nonaqueous synthesis and growth mechanism of AgCl/Ag, and its daylight-driven plasmonic photocatalysis. Chem Eur J 17:3710–3717
25. Chen DL, Yoo SH, Huang QS, Ali G (2012) Sonochemical synthesis of Ag/AgCl nano cubes and their efficient visible-light-driven photocatalytic performance. Chem Eur J 18:5192–5200
26. Liu L, Fu L, Liu Y, Jiang P (2009) Bioinspired synthesis of vertically aligned ZnO nanorod arrays: toward greener chemistry. Cryst Growth Des 9:4793–4796
27. Chen LY, Zhang ZD, Wang WZ (2008) Self-assembled porous 3D flowerlike β-In_2S_3 structures: synthesis, characterization, and optical properties. J Phys Chem C 112:4117–4123
28. Zuo F, Yan S, Zhang B, Zhao Y, Xie Y (2008) L-Cysteine-assisted synthesis of PbS nanocube-based pagoda-like hierarchical architectures. J Phys Chem C 112:2831–2835
29. Jiang JH, Yu RL, Yi R, Qin WQ, Qiu GZ (2010) Biomolecule-assisted synthesis of flower-like NiS microcrystals via a hydrothermal process. J Alloys Compd 493:529–593

30. Xiong SL, Xi BJ, Wang CM, Zou GF, Fei LF, Wang WZ, Qian YT (2007) Shape-controlled synthesis of 3D and 1D structures of CdS in a binary solution with L-Cysteine's sssistance. Chem Eur J 13:3076–3081
31. Jiang J, Li H, Zhang LZ (2012) New insight into daylight photocatalysis of AgBr@Ag: synergistic effect between semiconductor photocatalysis and plasmonic photocatalysis. Chem Eur J 18:6360–6369
32. Yu J, Dai G, Huang B (2009) Fabrication and characterization of visible-light-driven plasmonic photocatalyst Ag/AgCl/TiO_2 nanotube arrays. J Phys Chem C 113:16394–16401
33. Zhang Y, Tang Z, Fu X (2011) Nanocomposite of Ag-AgBr-TiO_2 as a photoactive and durable catalyst for degradation of volatile organic compounds in the gas phase. Appl Catal B 106:445–452
34. Chiu CK, Choi YJ, Luo TJM (2012) Formation of AgCl cubic crystals induced by shrinkage of sol-gel silica film. Cryst Growth Des 12:4727–4732
35. Wu QZ, Chen X, Zhang P, Han YC, Chen XM, Yan YH, Li SP (2008) Amino acid-assisted synthesis of ZnO hierarchical architectures and their novel photocatalytic activities. Cryst Growth Des 8:3010–3018
36. Jia CC, Yang P, Huang BB (2014) Uniform Ag/AgCl necklace-like nano-heterostructures: fabrication and highly efficient plasmonic photocatalysis. ChemCatChem 6:611–617
37. Xu H, Song YH (2012) Plasmonic-enhanced visible-light-driven photocatalytic activity of Ag-AgBr synthesized in reactable ionic liquid. J Chem Technol Biotechnol 87:1626–1633
38. Wang P, Huang BB, Lou ZZ (2010) Synthesis of highly efficient Ag@AgCl plasmonic photocatalysts with various structures. Chem Eur J 16:538–544
39. Li YY, Ding Y (2010) Porous AgCl/Ag nanocomposites with enhanced visible light photocatalytic properties. J Phys Chem C 114:3175–3179
40. Redmond PL, Brus LE (2007) 'Hot electron' photo-charging and electrochemical discharge kinetics of silver nanocrystals. J Phys Chem C 111:14849–14854
41. Luo G, Jiang X, Li M, Shen Q, Zhang Z (2013) Facile fabrication and enhanced photocatalytic performance of Ag/AgCl/rGO heterostructure photocatalyst. Appl Mater Interfaces 5:2161–2168
42. Li KX, Yan LS (2014) Fabrication of $H_3PW_{12}O_{40}$-doped carbon nitride nanotubes by one-step hydrothermal treatment strategy and their efficient visible-light photocatalytic activity toward representative aqueous persistent organic pollutants degradation. Appl Catal B 156–157:141–152
43. Tang YX, Jiang ZL, Xing GC, Li A (2013) Efficient Ag@AgCl cubic cage photocatalysts profit from ultrafast plasmon-induced electron transfer processes. Adv Funct Mater 33:2932–2940